


Projected climate variability of internal waves in the Andaman Sea

B. Yadidya¹   & A. D. Rao¹ 

The Andaman Sea, in the northeast Indian Ocean, is renowned for large-amplitude internal waves. Here, we use a global climate model (CanESM5) to investigate the long-term variability of internal waves in the Andaman Sea under a range of shared socioeconomic pathway (SSP) scenarios. SSPs are future societal development pathways related to emissions and land use scenarios. We project that mean values of depth-averaged stratification will increase by approximately 6% (SSP1-2.6), 7% (SSP2-4.5), and 12% (SSP5-8.5) between 1871-1900 and 2081-2100. Simulating changes in internal tides between the present (2015-2024) and the end-century (2091-2100), we find that the increase in stratification will enhance internal tide generation by approximately 4 to 8%. We project that the propagation of internal tides into the Andaman Sea and the Bay of Bengal will increase by 8 to 18% and 4 to 19%, respectively, under different SSP scenarios. Such changes in internal tides under global warming will have implications for primary production and ecosystem health not only in the Andaman Sea but also in the Bay of Bengal.

¹Centre for Atmospheric Sciences, Indian Institute of Technology Delhi, New Delhi 110016, India. ✉email: yadidyabadarvada@gmail.com

The vertical distribution of temperature, salinity, and pressure determines ocean stratification. In light of human-induced climate change significantly altering oceanic temperature and salinity distribution, it is expected that oceanic stratification will be affected^{1,2}. Global ocean stratification has increased by 0.9% per decade during 1960–2018³. The majority of the increase (71%) occurred in the upper 200 m of the ocean and was primarily caused by temperature changes, with salinity changes playing a minor role locally³. Internal waves (IW) form when perturbations in the stratified layer induce them to move up or down, and these perturbations encounter a restoring buoyancy force⁴. Internal tides (ITs) are IWs that oscillate at tidal frequencies. The vertical transfer of water, heat and other climatically relevant tracers in the ocean is driven by turbulent mixing from breaking oceanic IWs. As a result, IWs play a crucial role in controlling the movement and distribution of heat and carbon across the climate system^{5,6}.

The Andaman Sea is located on the northeastern side of the Indian Ocean (Fig. 1a, b), bordered on the west by an arc of islands stretching from northern Sumatra to the Irrawaddy delta (Fig. 1c). The monsoonal climate dominates the region, with the northeast or winter monsoon prevailing from December to March and the southwest or summer monsoon prevalent from June to September⁷. It receives a large volume of freshwater influx from the Irrawaddy and Salween rivers in the northern part⁸. Equatorial forcing dominates the mean coastal circulation in the Andaman Sea^{9,10}. It is also characterised by extraordinarily large-amplitude IWs^{11,12}. Semidiurnal ITs are the most energetic part of the entire IW spectrum in the Andaman Sea^{13–16}. Yadidya et al.¹⁶ suggested strong IT seasonal and spatial variability using in-situ observations and numerical model simulations. Moreover, the changes in stratification due to the effect of the Indian Ocean Dipole (IOD) modulates the interannual variability of IWs in this region¹⁷. The Andaman Sea's coral reefs have been regarded as being among the most diversified and vast in the Indian Ocean¹⁸. Roder et al.¹⁹ reported that IWs-exposed corals are more

heterotrophic and rich in nutrient concentrations. Nielsen et al.²⁰ observed maximum *Chla* and primary production where the pycnocline interacted with bottom topography. This interaction helped in sub-surface nutrient-rich water mixing with the surface layers suggesting that IWs can enhance primary and secondary productivity.

We used CanESM5 from CMIP6 model simulations (see 'Methods') to examine the long-term variability of IW activity in Historical (1850–2014) and future (2015–2100) scenarios, given the huge consequences that IWs can have on the bio-physical ecosystem of the Andaman Sea. Density stratification is used as a proxy for IW activity^{21,22} to quantify its long-term changes (see 'Methods'). We assess the impact of temperature and salinity on density stratification because both of them affect density^{16,17}. One of the most severe hazards to coral reefs caused by climate change is the increasing frequency of severe coral bleaching²³. Wyatt et al.²⁴ hypothesised that the effect of IWs on coral reefs could establish and sustain thermal refuges where heat stress and coral bleaching risk can be controlled. However, future implications will depend on how the IW climate responds to further warming and increasing ocean stratification. Therefore, numerical model simulations are used to estimate changes in the IT energetics between the present (2015–2024) and end-century (2091–2100) with changing stratification. Later, we also discuss their implications on the bio-physical environment.

Results

Changes in stratification. The long-term changes in the density stratification are evaluated based on the stratification anomalies computed with respect to the density stratification in the Historical simulations (Fig. 2a). Since 1850, the Andaman Sea's annual density stratification did not show any long-term variability until 2000. However, it has increased by 0.2 cph from 2000 to 2014 in the Historical. The future projections under different scenarios also indicate an increasing trend with stratification

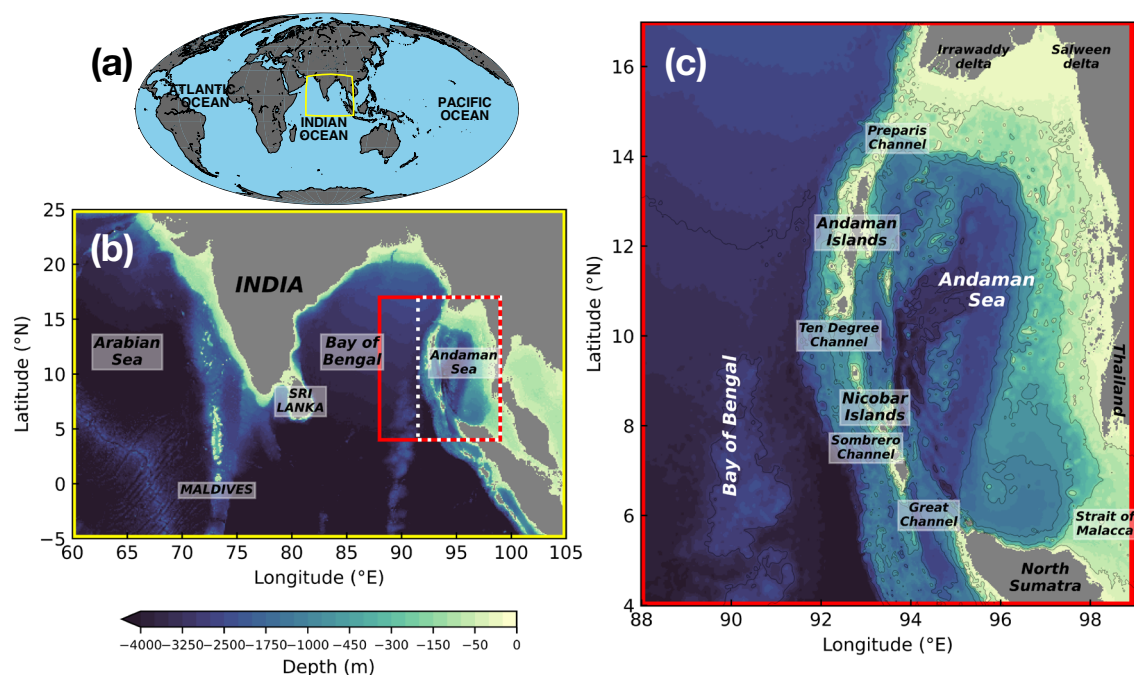


Fig. 1 Andaman Sea and model domain. a Global map highlighting the northern Indian Ocean region in yellow. The bathymetry of the (b) northern Indian Ocean and (c) the Andaman Sea is derived from GEBCO. The red box indicates the model domain, and the white box indicates the region over which the stratification is averaged (see 'Methods'). A non-linear colour bar is used. The appropriate copyright information for the GEBCO data are available at https://www.gebco.net/data_and_products/gridded_bathymetry_data/gebco_2019/grid_terms_of_use.html.

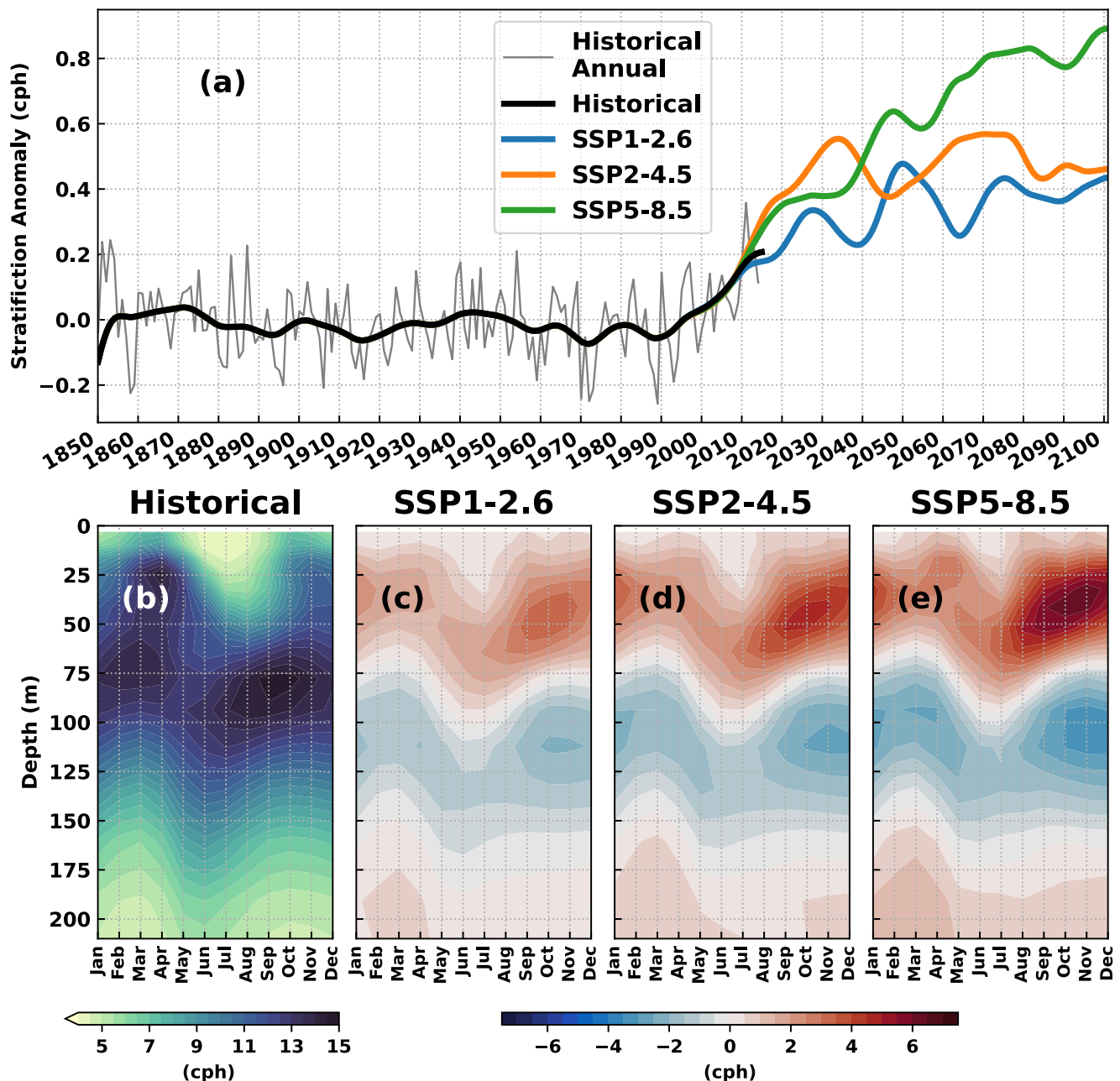


Fig. 2 Temporal changes in the Andaman Sea stratification. **a** Time series of Andaman Sea annual (grey) and 20-year low-pass filtered depth-averaged stratification anomalies relative to 1850–2014 mean derived from Historical (black), SSP1-2.6 (blue), SSP2-4.5 (orange), and SSP5-8.5 (green). **b** Annual cycle of the Andaman Sea stratification in Historical simulation. Annual cycle of stratification anomalies in **(c)** SSP1-2.6, **(d)** SSP2-4.5, and **(e)** SSP5-8.5 simulations relative to the annual cycle of Historical simulation. The Andaman Sea is represented by domain-averaged (4–17°N, 91.5–99°E) values (white box in Fig. 1b) derived from CanESM5.

increasing by 0.9 cph by the end-century under SSP5-8.5, which is the highest emissions no-policy baseline scenario. The Historical simulation's annual cycle of stratification profiles shows a bimodal signal with maximum stratification near 70–90 m (Fig. 2b). Strong positive (negative) anomalies are seen from 25 to 60 m (90–120 m), especially during boreal autumn and winter months, in all the SSP scenarios (Fig. 2c–e). This indicates a strong increase (decrease) in the stratification of the near-surface (sub-surface) waters in the coming years.

Furthermore, we investigated the relative contributions of variations in temperature and salinity to the trend in density stratification profiles on annual and seasonal timescales (Fig. 3). The corresponding profiles of salinity and temperature trends are

shown in Fig. 4. A three-layered trend pattern can be seen in the vertical (0–200 m), with a layer of decreasing trend sandwiched between two layers of an increasing trend in all the simulations. In the Historical (Fig. 3a), the first layer of increasing trend is seen up to 85 m, with the maximum (0.34 ± 0.14 cph/century) at 65 m. The layer of decreasing trend is present below that up to 185 m, with the maximum (-0.48 ± 0.12 cph/century) at 125 m. Increasing salinity (Fig. 4a) from 1850 to 2014 until 150 m resulted in salinity contributing to decreasing stratification trend (Fig. 3a). The effect of temperature is present throughout the water column, with temperature increasing from the surface to 70 m and below 125 m (Fig. 4e). Contrarily, salinity showed a decreasing trend from surface to 85 m in SSP1-2.6 (Fig. 4b),

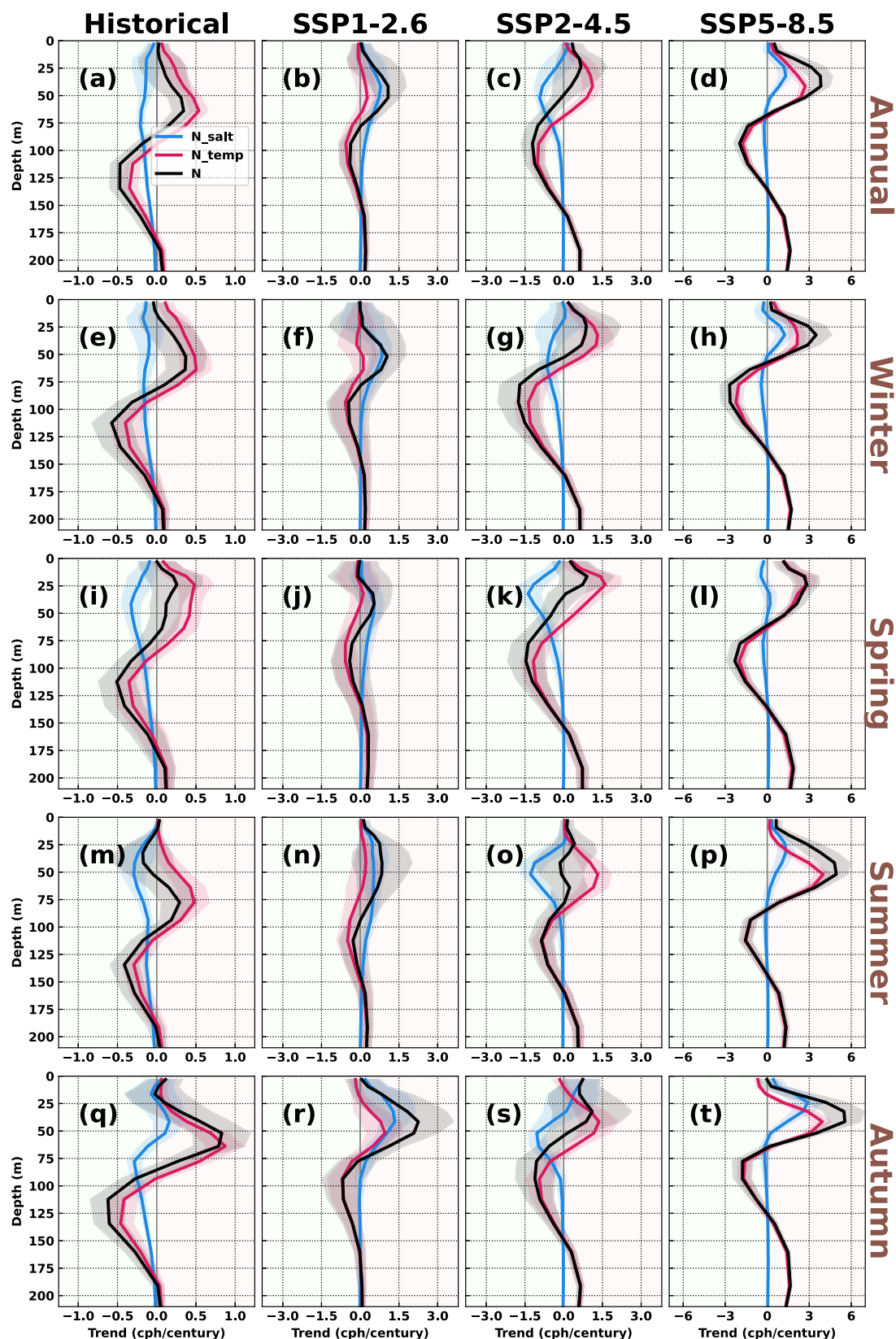


Fig. 3 Trend in the stratification profiles. The vertical profiles of linear trend (black) in density stratification in (a, e, i, m, q) Historical, (b, f, j, n, r) SSP1-2.6, (c, g, k, o, s) SSP2-4.5, and (d, h, l, p, t) SSP5-8.5 scenarios. Red and blue lines represent the effect of temperature and salinity on the stratification trend, respectively. The shaded region indicates the 95% confidence interval. Seasons are considered as follows: **e-h** winter is December-January-February, **i-l** spring is March-April-May, **m-p** summer is June-July-August, and **q-t** autumn is September-October-November.

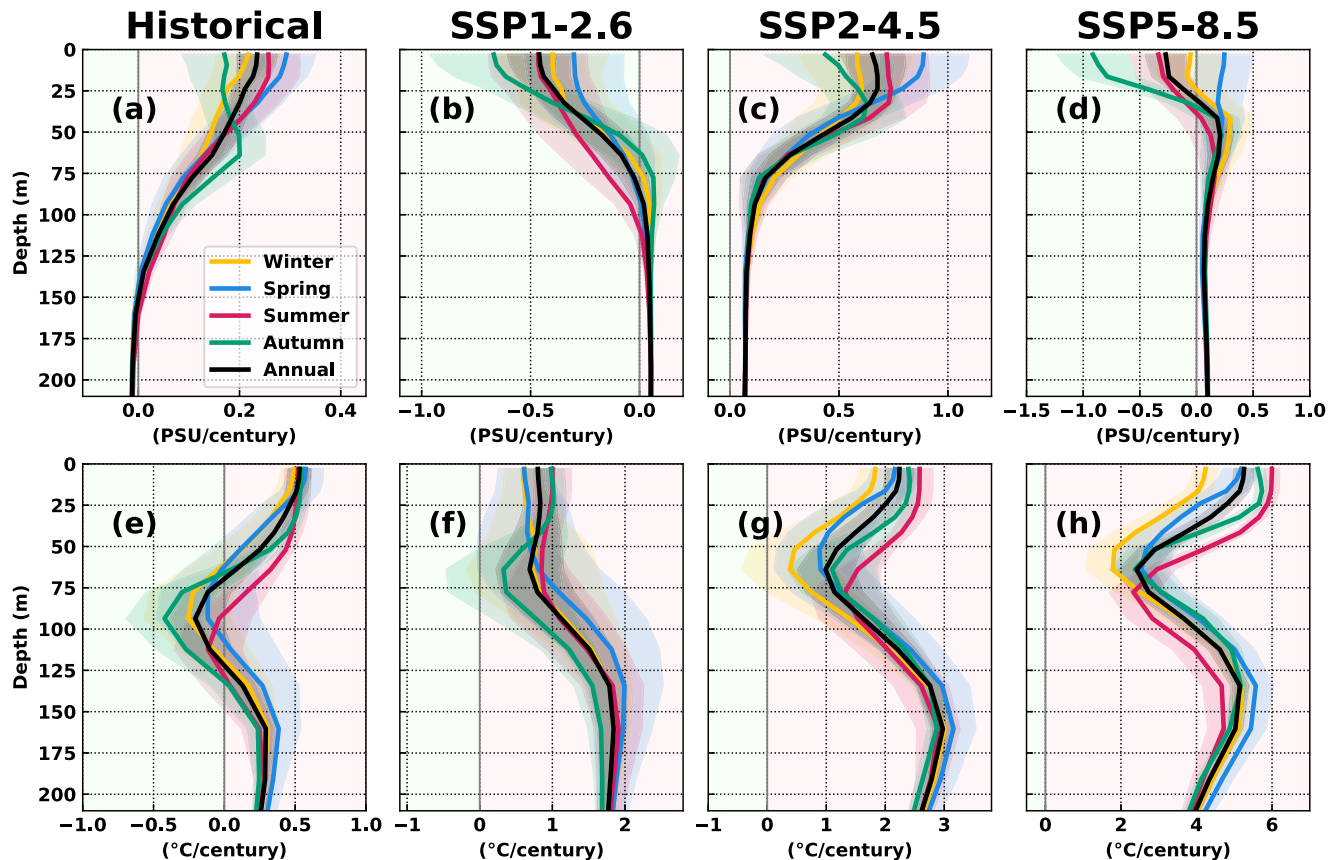


Fig. 4 Trend in the temperature and salinity profiles. The vertical profiles of a linear trend in (a–d) salinity and (e–h) temperature in (a, e) Historical, b, f SSP1-2.6, c, g SSP2-4.5, and (d, h) SSP5-8.5 scenarios. The shaded region indicates the 95% confidence interval.

which resulted in salinity influencing a strong increasing trend in stratification (Fig. 3b). In fact, the salinity effect dominates the first layer until 75 m, where a uniform increase in temperature is noticed (Fig. 4f). The temperature effect is present below 75 m leading to a decreasing trend up to 150 m. In the case of SSP2-4.5 (Fig. 3c), the impact of temperature and salinity in the near-surface layers is exactly the opposite. This has resulted in the shallowest increasing trend layer present only in the top 50 m. A thick layer of decreasing trend is observed from 50 to 150 m. A strong increase in both temperature (Fig. 4g) and salinity (Fig. 4c) in the near-surface layers has caused this to happen. In the extreme scenario of SSP5-8.5 (Fig. 3d), the stratification, fuelled by both temperature and salinity changes, is increasing from surface to 70 m, with the maximum increase (3.8 ± 0.65 cph/century) at 40 m. The decreasing trend layer is present from 70 to 140 m, below which the stratification increased strongly again.

In boreal winter, the Andaman Sea experiences the northeast monsoon associated with relatively strong precipitation and cooler temperatures near the surface, resulting in temperature inversions⁷. The vertical profiles of trends in Historical (Fig. 3e) and in all SSP scenarios (Fig. 3f–h) follow a similar pattern to that of annual (Fig. 3a–d). A strong decreasing trend in precipitation flux (Supplementary Fig. 1a) and water flux (Supplementary Fig. 1e) are observed in Historical, which could be contributing to increased salinity in the near-surface layers.

The Andaman Sea receives maximum insolation and net heat flux during spring (April and May). This results in the formation of the seasonal thermocline and shallow isothermal layer depth⁷. The maximum of the first layer of increasing trend (Fig. 3i–l) is very shallow compared to the annual (Fig. 3a–d). For example, in the Historical, it (0.25 ± 0.32 cph/century) is seen at 25 m during

spring but is at 65 m in annual. Moreover, there is a strong decreasing trend in water flux (Supplementary Fig. 1e–h) in all the experiments except SSP1-2.6 indicating excessive evaporation leading to high salinity in the near-surface waters. Therefore salinity effect shows a decreasing trend in stratification except in SSP1-2.6.

The onset of the southwest monsoon characterises the boreal summer season⁷. The precipitation flux (Supplementary Fig. 1a–d) and water flux (Supplementary Fig. 1e–h) showed the least variability among all seasons except in SSP1-2.6, where both showed an increasing trend. The salinity trend (Fig. 4a–d) is closest to the annual trend, whereas the temperature (Fig. 4e–h) showed the maximum increasing trend in the near-surface (up to 75 m). Regarding the trend in stratification (Fig. 3m–p), the Historical trend showed a four-layer pattern with an additional decreasing trend near the surface. This is caused due to uniform increase in temperature until 50 m and a strong decreasing trend effect by salinity. The maximum (4.9 ± 0.81 cph/century) of the increasing trend in the near-surface is the second-highest among all the seasons in SSP5-8.5.

During autumn, the northern part of the Andaman Sea receives a massive amount of freshwater influx from the Irrawaddy and Salween rivers⁸. The trend in water flux (Supplementary Fig. 1e–h) shows that the river runoff has increased in the Historical and is expected to increase in SSP2-4.5 and SSP5-8.5 scenarios. Furthermore, the precipitation flux (Supplementary Fig. 1a–d) shows a strong increasing trend in SSP2-4.5 and SSP5-8.5. The effect of this can be seen in the salinity trends (Fig. 4a–d), where the lowest increasing trend is seen in Historical and SSP2-4.5; and the largest decreasing trend in SSP1-2.6 and SSP2-4.5. The effect of both temperature and

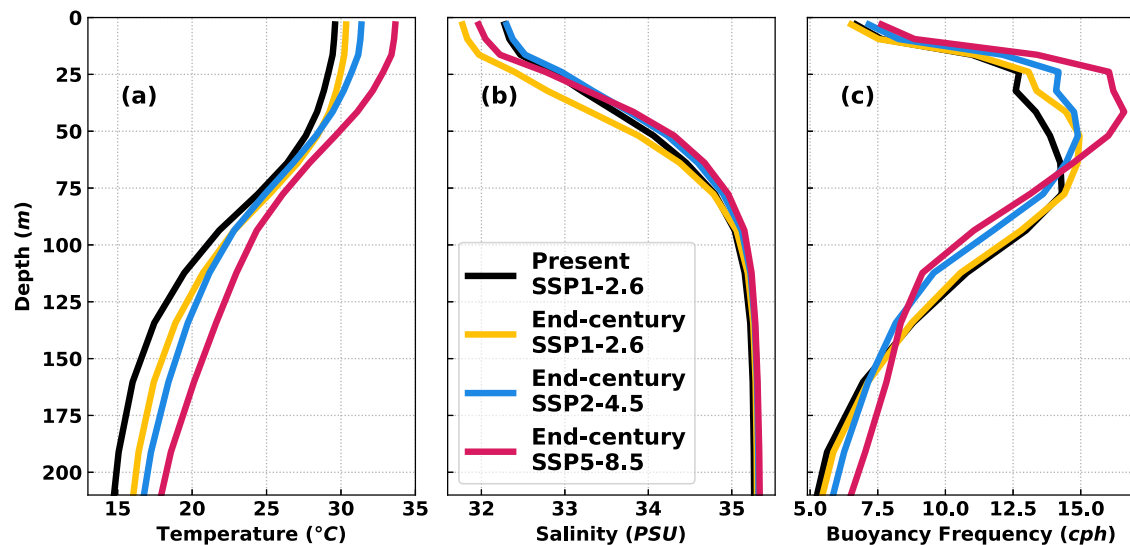


Fig. 5 Initial profiles used in numerical model simulations. Mean profiles of (a) temperature, (b) salinity and (c) buoyancy frequency used for model initialisation in four experiments to study the differences in IT generation, propagation, and dissipation between the present (2015–2024) and end-century (2091–2100).

salinity results in the highest increasing trend (maximum of 0.83 ± 0.36 , 2.25 ± 1.37 , 1.1 ± 1.52 , 5.54 ± 1.13 cph/century) in the first layer of near-surface waters in all the experiments (Historical, SSP1-2.6, SSP2-4.5, SSP5-8.5) (Fig. 3q–t). This shows that the increasing trend in stratification is highest during autumn and will continue to be during the same season in the future as well.

In summary, the density stratification trend profile shows a three-layer structure in the upper 200 m, with two layers of increasing trend separated by a layer of decreasing trend. It showed significant seasonal variability due to the combined effect of temperature and salinity. Under SSP1-2.6, in which the long-term estimate is projected to increase global warming by 1.8°C^{25} , the stratification increase is caused by salinity changes with no net effect from temperature changes. Contrarily, the salinity changes induced a negative effect on increasing stratification, which is completely fuelled by the temperature changes in SSP2-4.5 (long-term estimate of an increase by 2.7°C^{25}). In the high-end scenario of SSP5-8.5, where an increase of 4.4°C is expected by 2100²⁵, both temperature and salinity changes are contributing to the stratification increase. The depth-averaged stratification shows an increasing trend of 0.014 ± 0.04 , 0.21 ± 0.12 , 0.06 ± 0.11 , and 0.73 ± 0.11 cph/century under Historical (1850–2014), SSP1-2.6, SSP2-4.5, and SSP5-8.5 scenarios (2015–2100), respectively. The time series of density stratification profiles shown in Supplementary Fig. 2 reveals the same. For instance, in the Historical, the maximum buoyancy frequency was mostly less than 14 cph at 75 m. Whereas in SSP5-8.5, it is exceeding 16 cph at 45 m. The upwelling of highly stratified layers is also clearly seen in all the SSP scenarios.

Comparison of baroclinic tidal energy budget between the present and future. This section considers the mean stratification from 2015 to 2024 in SSP1-2.6 as the ‘present’ stratification. On the other hand, the mean stratification from 2091 to 2100 is considered as the ‘end-century’ stratification and is taken for SSP1-2.6, SSP2-4.5 and SSP5-8.5 scenarios. These two time periods are selected to evaluate and quantify the effect of increasing stratification from the present decade to the final decade in the CMIP6 (CanESM5) simulations on the IT energy budget. The temperature and salinity profiles and the corresponding density

stratification used for model initialisation are shown in Fig. 5. In the present SSP1-2.6, the buoyancy frequency increased until 75 m and gradually decreased below this depth. In different SSP scenarios, the end-century stratification is higher in the near-surface layers but is less than the present from 70–80 to 150–160 m. The changes in the IT energy budget (see ‘Methods’) comprising of IT generation, propagation, and dissipation from the present to the end-century are discussed in detail (Fig. 6). Six sub-regions (Fig. 6a) are selected for this analysis where the IT generation is relatively high^{16,17}.

In the Preparis Channel (PC), located in the northwestern Andaman Sea, the IT generation changed very little in the SSP1-2.6 (Fig. 6b, c) and SSP2-4.5 (Fig. 6b, d) scenarios but increased by 9% in SSP5-8.5 (Fig. 6b, e). However, the westward propagation of IT into the Bay of Bengal and eastward propagation into the Andaman Sea is seen to increase by 1.2–17.5% and 8–16.2% in different scenarios. The baroclinic energy conversion in the Ten Degree Channel (TDC), located between the Andaman and Nicobar Islands, could increase by 2.9–9.2%. The local dissipation ratio in present is 0.53 (Fig. 6b) but is projected to decrease by 17.3–25.1% (Fig. 6c–e). The decrease in dissipation could result in increased baroclinic flux into both Bay of Bengal and the Andaman Sea, but more so into the latter by 19–33.9% (Fig. 6c–e).

Sombrero Channel (SC) is the main generation site for IT in the Andaman Sea. The IT generation is found to be almost the same in the SSP1-2.6 (Fig. 6b, c) and SSP2-4.5 (Fig. 6b, d) scenarios but could decrease by 6.7% in SSP5-8.5 (Fig. 6b, e). The propagation of IT also showed the least amount of variability in the SSP1-2.6 and SSP2-4.5 but could increase by 4.9% and 12.6% in the Bay of Bengal and Andaman Sea in SSP5-8.5, respectively. However, the local dissipation ratio could decrease by 9.6–62.3% (Fig. 6c–e) from 0.15 (Fig. 6b). The Great Channel (GC) is the southernmost channel between the Nicobar Islands and North Sumatra. The barotropic to baroclinic energy conversion is predicted to increase by 13.8–24.2%. The local dissipation efficiency ratio increased by 27.2% (Fig. 6c) and 13.2% (Fig. 6d) but decreased by 21.3% (Fig. 6e) from 0.24 (Fig. 6b) in SSP1-2.6, SSP2-4.5, and SSP5-8.5, respectively. This increased the IT propagation into the Bay of Bengal by 17.5–91%.

The generation of IT in the North East Andaman Sea (NEAS) increased by 4.1–10.1%. However, a massive increase is seen in

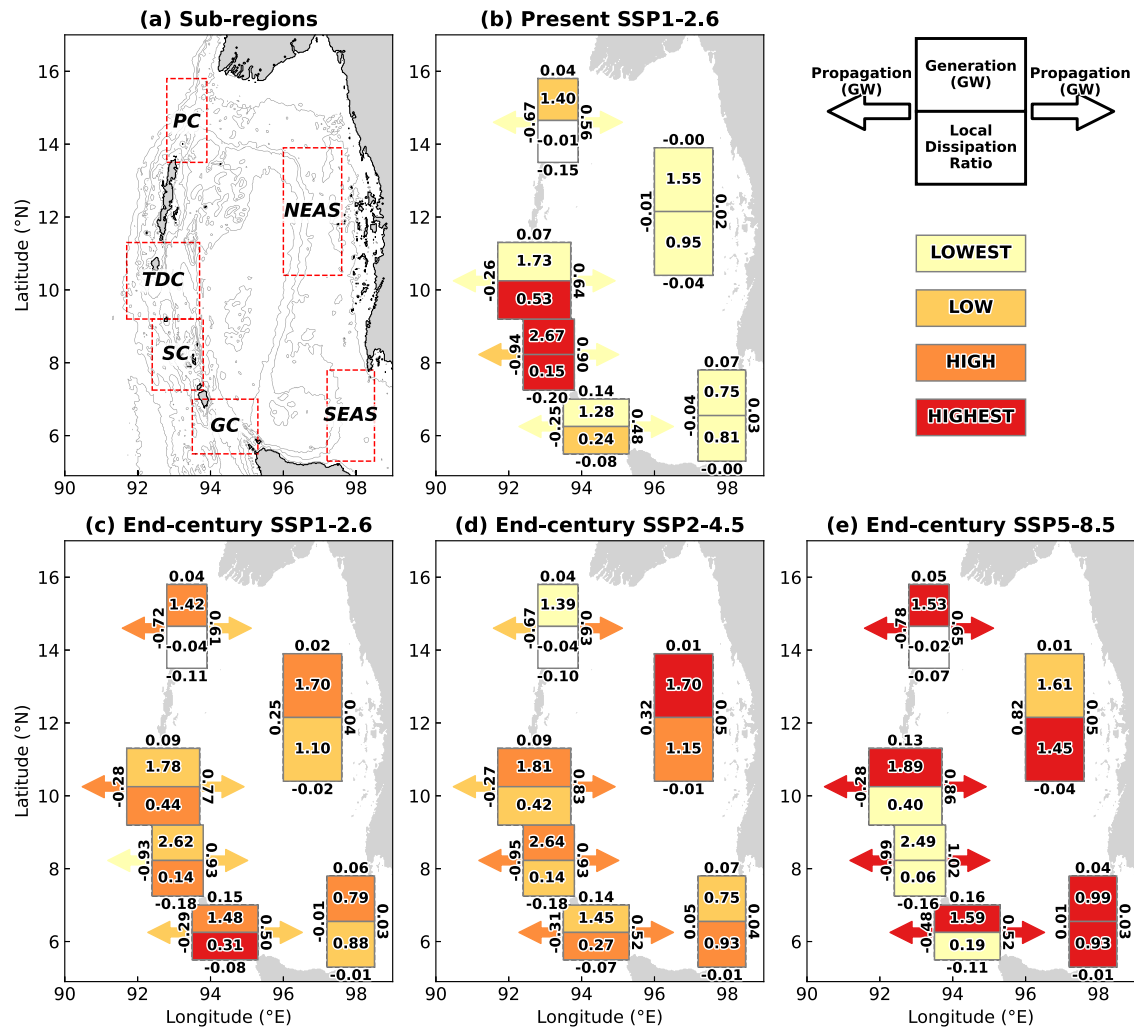


Fig. 6 Internal tide energy budget in the present and end-century. **a** Bathymetry of the Andaman Sea denoting the sub-regions where IT energetics are discussed. Comparison of IT energy budget between **(b)** the present (SSP1-2.6) and **(c–e)** end-century under **(c)** SSP1-2.6, **d** SSP2-4.5 and **(e)** SSP5-8.5 scenarios. The top half in each sub-region indicates region-integrated and depth-integrated IT energy conversion rate (GW), whereas the bottom half reflects the local dissipation ratio. The depth-integrated baroclinic energy fluxes (GW) are shown along the boundaries. Positive numbers along the boundaries denote propagation towards the north and east, whereas negative numbers indicate southward and westward propagation.

the IT propagating into NEAS by 68.9–98% from the western side. This is mainly due to the increased baroclinic flux into the Andaman Sea at PC, TDC, and SC. The local dissipation ratio also increases from 0.95 (Fig. 6b) to 1.1–1.45 (Fig. 6c–e), an increase of 15.3–52.6%. The ratio >1 indicates remote dissipation of IT. In the South East Andaman Sea (SEAS) region, which connects the Andaman Sea to the Malacca Strait, the IT generation increased by 31.9% in SSP5-8.5 (Fig. 6e) but is relatively similar in the other two scenarios (Fig. 6c, d). On the other hand, the local dissipation efficiency increased from 0.81 to 0.88–0.93 (8.6–15%).

The model simulations suggest that the amount of IT generated is increasing in most of the generation sites with changing stratification. The mean energy conversion of the six main generation sites increased by 4.4%, 4.05%, and 7.66% under SSP1-2.6, SSP2-4.5, and SSP5-8.5 scenarios, respectively. The local dissipation in the western Andaman Sea is also decreasing significantly. Therefore, a sharp increase in the baroclinic energy flux into the Bay of Bengal (4.19–19.25%); and into the Andaman Sea (7.95–18.05%) is noticed. Consequently, the eastern Andaman Sea is receiving high IT flux resulting in high remote dissipation of IT.

Discussion and conclusions

IW activity in the Andaman Sea has been influenced by changes in density stratification caused due to climate change and has increased since the turn of the century. Under future SSP scenarios, changes in temperature and salinity result in increased density stratification, especially in the near-surface waters where the euphotic zone exists. Boreal autumn is expected to see the maximum increase in stratification when the IOD's effect is maximum. The Andaman Sea is quite distinct from other regions like South China Sea, where large-amplitude IWs are present. It is unique due to the presence of a double pycnocline, where the stratification of density is affected by both temperature and salinity^{16,17,26}. Li et al.³ reported that during 1960–2018, > 90% of the increase in stratification is caused by temperature changes in the global oceans. However, in the Andaman Sea, we found that salinity changes are also important along with temperature changes in both Historical and future SSP scenarios. For example, increasing salinity of the near-surface waters in SSP2-4.5, with intermediate greenhouse gas emissions, leads to a negative effect on the increasing stratification from 2015 to 2100. Whereas in the other two scenarios, i.e., SSP1-2.6 and SSP5-8.5, which are on either end of the spectrum in terms of emissions, decreasing

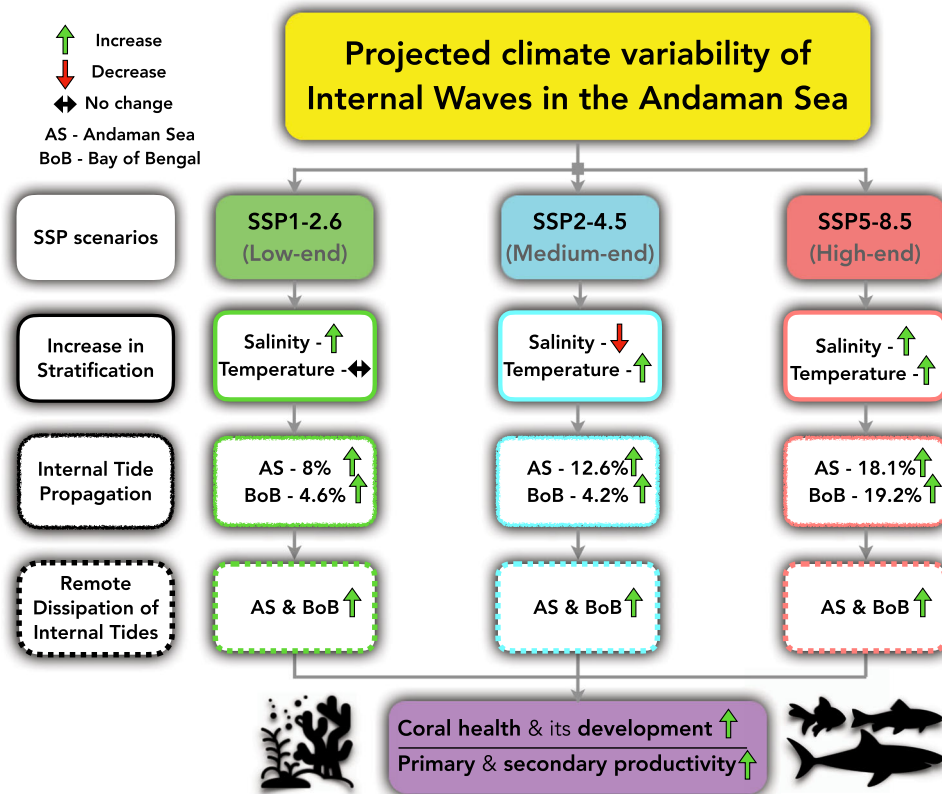


Fig. 7 Schematic diagram summarising the projected climate variability of internal waves in the Andaman Sea. The second row represents the different SSP scenarios. The effect of salinity and temperature on the increasing stratification trend is shown in the third row. The ‘increase’ (‘decrease’) sign in this column indicates that the salinity/temperature changes contribute to an increase (decrease) in stratification. The ‘no change’ icon indicates that the salinity/temperature has little to no effect on changing stratification. In the fourth and fifth row, the increase in the IT propagation into the Andaman Sea (AS) and Bay of Bengal (BoB) and subsequent increase in remote dissipation simulated by MITgcm between the present (2015–2024) and the end-century (2091–2100) is shown. The potential implications are shown in the sixth and final row.

salinity has a positive effect on the increasing stratification. The signal-to-noise ratio between different realisations of CanESM5 in Supplementary Fig. 3 also shows that the uncertainty in salinity changes is high within the top 30 m in all the SSP scenarios. However, the mechanisms for the differences in salinity changes between the SSP scenarios are beyond the scope of this study but could be due to changes in the river runoff, precipitation, evaporation, and the dynamical processes related to them.

Even though the effect of salinity and temperature changes is different between different SSP scenarios, their cumulative effect has resulted in increasing stratification in all the cases. Therefore, we carried out model simulations using MITgcm to quantify and evaluate the changes in IT energy budget between the first and last decades of SSP simulations. We assumed that the first decade (2015–2024) is best represented by the SSP1-2.6, which is the low end of the range of potential future pathways, and considered the mean stratification to represent the ‘present’. Later, we compared the results from the ‘present’ to ‘end-century’ (2091–2100) of all the three SSP scenarios consisting of the low end (SSP1-2.6), the medium part (SSP2-4.5), and the high end (SSP5-8.5) of the range of future pathways in terms of emissions and global temperature rise²⁷.

The model simulations suggested a significant increase in the IT generation and propagation into the Andaman Sea by the end-century. The increase in IT generation and associated dissipation can influence the large-scale ocean circulation in the northern Indian Ocean²⁸. The resultant changes in the IW field could play a significant, though underappreciated, role in increasing primary productivity; and protecting diverse coral reefs. Increasing

diapycnal mixing as a result of increased dissipation rates would boost the supply of nutrients and plankton that aid in the development of coral reef²⁹. Thermal stress in the future SSP scenarios is three to four times higher than it is now, posing a serious threat to the health of future reef ecosystems³⁰. The increase in the propagation of ITs into the Andaman Sea could provide much-needed thermal relief to the diverse corals present in this region. By regularly flushing reefs with cooler water, IWs can alter species assemblages³¹, alleviate thermal stress³², and lower corals’ vulnerability to bleaching^{24,33}. Recent observations^{34,35} and modelling studies³⁶ indicated the IWs generated in the Andaman Sea can travel as far as the east coast of India, Sri Lanka and Maldives. They contribute to vertical mixing near the coasts, where the IWs break and release their energy. The local dissipation in the western Andaman Sea has decreased significantly in the end-century simulations. Hence, the increase in the baroclinic flux into the Bay of Bengal from PC, TDC, SC and GC can contribute to reducing the thermal stress on remote coral reefs present in the coastal waters of Maldives, Sri Lanka and the east coast of India.

Field measurements in the northern South China Sea revealed that the dissipation of IWs led to the pumping of nutrients to the oligotrophic surface water, thereby causing a rapid increase of phytoplankton³⁷. The increased dissipation and mixing in the eastern Andaman Sea and the Bay of Bengal could enhance primary and secondary productivity^{20,38}. Muacho et al.³⁹ also suggested that IWs can increase the amount of carbon uptake, thereby enhancing the primary production on 3 to 4-day time-scales. In addition to boosting marine production through

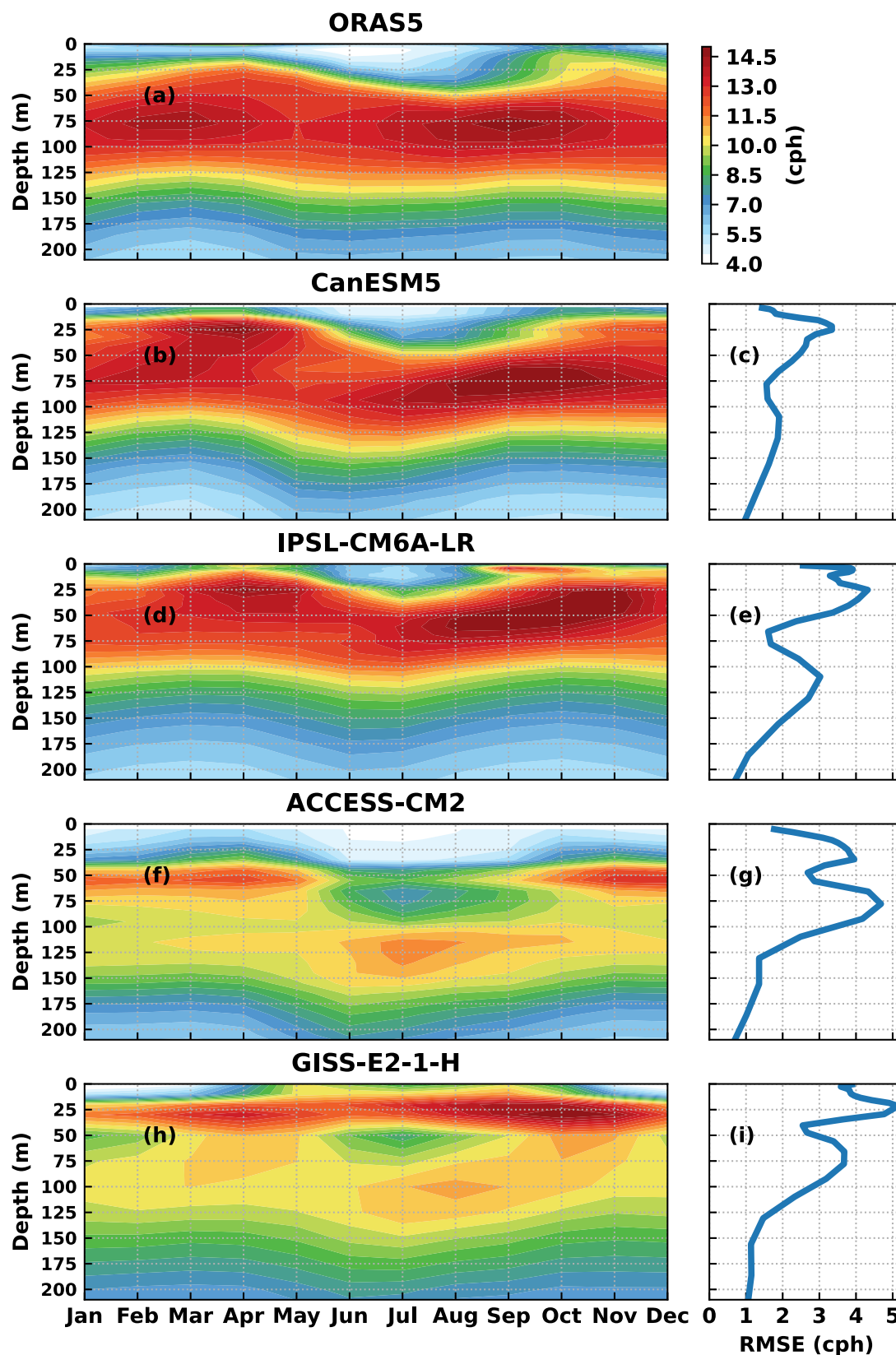


Fig. 8 Validation of CMIP6 data. Comparison of the annual cycle of density stratification profiles in the Andaman Sea between (a) ORAS5 and historical simulations of (b) CanESM5, d IPSL-CM6A-LR, f ACCESS-CM2, h GISS-E2-1-H during 1993–2015. The root mean square error (RMSE) of monthly stratification at different depths between ORAS5 and CanESM5, IPSL-CM6A-LR, ACCESS-CM2, GISS-E2-1-H is shown in (c, e, g, i), respectively.

mixing, IWs can directly transfer a large volume of nutrients and chemicals.

The schematic diagram shown in Fig. 7 summarises this study. We found that the salinity and temperature changes play different roles on increasing stratification in different SSP scenarios from 2015 to 2100. Model simulations showed some interesting results where a significant increase in the IT generation in the Andaman Sea led to an increase in the IT propagation into both the Andaman Sea and Bay of Bengal. Consequently, the remote dissipation in both the Andaman Sea and Bay of Bengal are projected to increase. Subsequently, we discussed the potential implications of the increased stratification and IW activity on the vast and diverse coral reefs in the northern Indian Ocean. We also suggest that the enhanced mixing could potentially increase marine productivity in this region. This study's results can be a vital tool for coral reef conservation and management in a warming ocean.

Methods

Data sources and processing. The interannual variability in the equatorial Indian Ocean is primarily driven by the IOD⁴⁰, which is a coupled ocean and atmospheric phenomenon. A positive IOD is characterised by warm sea surface temperature anomalies on the western side of the equatorial Indian Ocean and vice versa on the eastern side. On the other hand, warm waters are present on the eastern side during a negative IOD event. According to ref. ⁴¹, the following CMIP6 models were able to simulate the dynamics of the IOD, which largely influences the Andaman Sea stratification¹⁷, reasonably well. They are CanESM5, IPSL-CM6A-LR, ACCESS-CM2, and GIDD-E2-1-H. The annual cycle of buoyancy stratification of these four global climate models during 1993–2014 is compared with Ocean Reanalysis System 5⁴² (ORAS5) data in Fig. 8. The root mean square error (RMSE) between the time series of ORAS5 stratification and the four CMIP6 models is also shown. CanESM5 (r1i1p2f1) is the most accurate in capturing the annual cycle and the depths of maximum stratification among the four models. The vertical profiles of RMSE also show the least error in CanESM5. Maximum RMSE at 25 m could be due to overestimation of stratification due to seasonal or secondary thermocline during the spring season.

The Historical experiment and three Shared Socioeconomic Pathways (SSPs) scenarios (SSP1-2.6, SSP2-4.5 and SSP5-8.5) are chosen from CanESM5 in this study²⁷. SSP1-2.6 reflects the low end of the range of potential future forcing pathways and updates the RCP2.6 (Representative Concentration Pathway) from CMIP5. It combines low vulnerability, less obstacles for mitigation, and a low forcing signal to create a multi-model mean warming by 2100 that is predicted to be much less than 2 °C. SSP2-4.5 represents the medium part of the range of future forcing pathways which combines intermediate societal vulnerability and intermediate forcing level. It is an update of the RCP4.5 pathway. SSP5-8.5 is the high end of the range of future pathways and an update of RCP8.5, which produces a radiative forcing of 8.5 W/m² in 2100. All computations and analyses were carried out in Python on the cloud-based computing platform *Pangeo*. This study's workflow makes use of *xarray*^{43,44}, *dask*⁴⁵, *xgcm*⁴⁶, *xmitgcm*⁴⁷, *xesmf*⁴⁸ and *xmip*⁴⁹.

Density stratification and internal waves. The generation of IWs (conversion of barotropic tides to baroclinic motions) is directly proportional to N^2 , as shown by the equation of 'Baines force', F_B , in ref. ²² given as

$$F_B = N^2 w_{bt} \omega_{bt}^{-1} \quad (1)$$

where g is gravitational acceleration, ρ is density, ρ_0 is background density, z is depth, w_{bt} is the vertical barotropic velocity, ω_{bt} is the barotropic tidal frequency, and N is the Brunt–Väisälä buoyancy frequency given by

$$N = \sqrt{-\frac{g}{\rho_0} \frac{\partial \rho}{\partial z}} \quad (2)$$

Therefore, increased density stratification in the pycnocline increases IW generation by the barotropic tide. Numerical studies carried out in the Andaman Sea^{14,16} and the Luzon Strait^{50,51}, two of the most active IW generation sites in the world oceans, support this theory. The Andaman Sea stratification (N) is represented by domain-averaged (4–17°N, 91.5–99°E) values.

Quantifying the effect of temperature and salinity on stratification. The influence of temperature and salinity on the Andaman Sea stratification (N) can be assessed independently by using climatological means for one variable and varying the other variable. To accomplish this, we computed N_{temp} (N_{salt}) using climatological monthly mean salinity (temperature) and varying temperature (salinity) from CMIP6 data.

Computation of linear trends. Ordinary least-squares linear regression was performed to assess statistically significant trends ($P < 0.05$) in stratification (N) with respect to time for both the seasonal and annual time series under consideration following ref. ²². The same procedure is repeated for N_{temp} and N_{salt} to quantify the trend in stratification (N) due to temperature and salinity alone, respectively. The 95% confidence interval is shown by error bars throughout this study to indicate the level of uncertainty in the linear trends³.

Model configuration. This research employs a three-dimensional, z-coordinate, hydrostatic/nonhydrostatic finite-volume model, Massachusetts Institute of Technology General Circulation Model⁵² (MITgcm), that solves the incompressible Navier–Stokes equations on an Arakawa-C grid using the Boussinesq approximation. Figure 1 shows the model bathymetry from the General Bathymetric Chart of the Oceans⁵³ (GEBCO). The model domain spans the entire Andaman Sea from 4°N to 17°N and 88°E to 99°E⁵⁴. Grid spacing is 2.7 km in both zonal and meridional directions. The simulations are done in the hydrostatic mode. There are 48 levels in the vertical direction. The thickness of vertical levels is 5 m in the top 150 m, and it steadily decreases below that. The Smagorinsky formulation⁵⁵ (K-profile parameterisation scheme) parameterises the horizontal (vertical) eddy viscosity and diffusivity. No-slip and free-slip conditions are implemented to the bottom and lateral boundaries. The bottom drag coefficient is set to a constant of 0.0025.

The semidiurnal ITs dominate the IW spectrum in this region¹⁶. Therefore, the amplitudes and phases of semidiurnal (M_2 , S_2) barotropic tides extracted from the TOPEX/Poseidon global tidal model⁵⁶ (TPXO9.2) are used to force the model at the open boundaries. Along each open boundary, a 0.25°-thick sponge layer is applied to reduce artificial reflections and absorb waves that propagate out of the model domain. The spatially homogenous temperature and salinity profiles used for model initialisation are shown in Fig. 5. Four experiments, i.e., 'Present SSP1-2.6', 'End-century SSP1-2.6', 'End-century SSP2-4.5', and 'End-century SSP5-8.5', are carried out, and their IT energetics are discussed. This model configuration is already tested and validated by Yadidya et al.^{16,17} for studying the seasonal and interannual variability of ITs in the Andaman Sea. The model is run for four weeks in all the simulations, and the last 2 weeks' data are analysed.

Estimation of IT energetics. The IT energy budget analysis^{57,58} is carried out by neglecting the tendency and advection terms as a first-order approximation and is defined as:

$$\langle DIS_{bc} \rangle = \langle Conv \rangle - \langle DIV_{bc} \rangle \quad (3)$$

where DIS_{bc} is the depth-integrated dissipation rate of internal tides, $Conv$ is the depth-integrated conversion rate of barotropic-to-baroclinic energy, and DIV_{bc} is the depth-integrated divergence flux of internal tides. A 14-day average, denoted by the angle bracket, is taken to eliminate the effects of intratidal and neap-spring variability^{15,59}.

$$Conv = g \int_{-H}^{\eta} \rho' w_{bt} dz \quad (4)$$

$$DIV_{bc} = \nabla_h \cdot \left[\int_{-H}^{\eta} u' p' dz \right] \quad (5)$$

where H is the time-mean water depth, η is the surface tidal elevation, ρ' represents the density perturbation, w_{bt} is the barotropic vertical velocity, u' and p' are the baroclinic components of tidal velocity and pressure perturbation, respectively. The pressure perturbations are derived from the density anomalies following ref. ⁵⁸

$$p'(z, t) = -\frac{1}{H} \int_{-H}^{\eta} \int_z^{\eta} g \rho'(\tilde{z}, t) d\tilde{z} dz + \int_z^{\eta} g \rho'(\tilde{z}, t) d\tilde{z} \quad (6)$$

The local dissipation efficiency, q , is the ratio of the area-integrated baroclinic dissipation rate and area-integrated barotropic-to-baroclinic energy conversion rate⁶⁰,

$$q = \frac{\int_s ds \langle DIS_{bc} \rangle}{\int_s ds \langle Conv \rangle} \quad (7)$$

Data availability

Data relevant to this study can be downloaded from the websites listed below: ORAS5 at <https://resources.marine.copernicus.eu/>; CMIP6 database at <https://esgf-node.llnl.gov/projects/cmip6/>, Searchable keywords: 'CanESM5', 'IPSL-CM6A-LR', 'ACCESS-CM2', 'GIDD-E2-1-H'.

Code availability

The python codes used in this study are available upon request.

Received: 5 May 2022; Accepted: 5 October 2022;

Published online: 28 October 2022

References

- Durack, P. J. Ocean salinity and the global water cycle. *Oceanography* **28**, 20–31 (2015).
- Cheng, L., Abraham, J., Hausfather, Z. & Trenberth, K. E. How fast are the oceans warming? *Science* **363**, 128–129 (2019).
- Li, G. et al. Increasing ocean stratification over the past half-century. *Nat. Clim. Change* **10**, 1116–1123 (2020).
- Garrett, C. & Munk, W. Space-time scales of internal waves: a progress report. *J. Geophys. Res.* **80**, 291–297 (1975).
- Whalen, C. B. et al. Internal wave-driven mixing: governing processes and consequences for climate. *Nat. Rev. Earth Environ.* **1**, 606–621 (2020).
- MacKinnon, J. A. et al. Climate process team on internal wave-driven ocean mixing. *Bull. Am. Meteorol. Soc.* **98**, 2429–2454 (2017).
- Varkey, M. J., Murty, V. S. N. & Suryanarayana, A. Physical oceanography of the Bay of Bengal and Andaman Sea. *Oceanography Marine Biol. Annu. Rev.* <https://www.vliz.be/en/imis?refid=27018> (1996).
- Robinson, R. et al. The Irrawaddy river sediment flux to the Indian ocean: the original nineteenth-century data revisited. *J. Geol.* **115**, 629–640 (2007).
- Webster, P. J., Moore, A. M., Loschnigg, J. P. & Leben, R. R. Coupled ocean-atmosphere dynamics in the Indian Ocean during 1997–98. *Nature* **401**, 356–360 (1999).
- Chatterjee, A., Shankar, D., McCreary, J. P., Vinayachandran, P. N. & Mukherjee, A. Dynamics of Andaman Sea circulation and its role in connecting the equatorial Indian Ocean to the Bay of Bengal. *J. Geophys. Res.: Oceans* **122**, 3200–3218 (2017).
- Perry, R. B. & Schimke, G. R. Large-amplitude internal waves observed off the northwest coast of Sumatra. *J. Geophys. Res.* **70**, 2319–2324 (1965).
- Osborne, A. R. & Burch, T. L. Internal solitons in the Andaman Sea. *Science* **208**, 451–460 (1980).
- Mohanty, S., Rao, A. D. & Latha, G. Energetics of semidiurnal internal tides in the Andaman Sea. *J. Geophys. Res.: Oceans* **123**, 6224–6240 (2018).
- Jithin, A., Francis, P., Unnikrishnan, A. & Ramakrishna, S. Energetics and spatio-temporal variability of semidiurnal internal tides in the Bay of Bengal and Andaman Sea. *Progr. Oceanography* **189**, 102444 (2020).
- Peng, S. et al. Energetics-based estimation of the diapycnal mixing induced by internal tides in the Andaman Sea. *J. Geophys. Res.: Oceans* **126**. <https://doi.org/10.1029/2020JC016521> (2021).
- Yadidya, B., Rao, A. D. & Latha, G. Investigation of internal tides variability in the Andaman Sea: observations and simulations. *J. Geophys. Res.: Oceans* **127**, e2021JC018321 (2022).
- Yadidya, B. & Rao, A. D. Interannual variability of internal tides in the Andaman Sea: an effect of Indian Ocean Dipole. *Sci. Rep.* **12**, 11104 (2022).
- Wallace, C. C. & Muir, P. R. Biodiversity of the Indian Ocean from the perspective of staghorn corals (*Acropora* spp.). *INDIAN J. MAR. SCI.* **34**, 8 (2005).
- Roder, C. et al. Trophic response of corals to large amplitude internal waves. *Marine Ecol. Progr. Ser.* **412**, 113–128 (2010).
- Nielsen, T. et al. Hydrography, bacteria and protist communities across the continental shelf and shelf slope of the Andaman Sea (NE Indian Ocean). *Marine Ecol. Progr. Ser.* **274**, 69–86 (2004).
- Baines, P. G. On internal tide generation models. *Deep Sea Res. Part A. Oceanographic Res. Papers* **29**, 307–338 (1982).
- DeCarlo, T. M., Karnauskas, K. B., Davis, K. A. & Wong, G. T. F. Climate modulates internal wave activity in the Northern South China Sea. *Geophys. Res. Lett.* **42**, 831–838 (2015).
- van Hooijdonk, R. et al. Local-scale projections of coral reef futures and implications of the Paris Agreement. *Sci. Rep.* **6**, 39666 (2016).
- Wyatt, A. S. J. et al. Heat accumulation on coral reefs mitigated by internal waves. *Nat. Geosci.* **13**, 28–34 (2020).
- Masson-Delmotte, V. et al. Climate change 2021: the physical science basis. In *Contribution of working group I to the sixth assessment report of the intergovernmental panel on climate change* Vol. 2 (Cambridge University Press Cambridge, UK, 2021).
- Silva, J. C. B. d. & Magalhaes, J. M. Internal solitons in the Andaman Sea: a new look at an old problem. in *Remote Sensing of the Ocean, Sea Ice, Coastal Waters, and Large Water Regions 2016*, Vol. 9999, 42–54 (SPIE, 2016).
- O'Neill, B. C. et al. The scenario model intercomparison project (ScenarioMIP) for CMIP6. *Geosci. Model Dev.* **9**, 3461–3482 (2016).
- Wunsch, C. & Ferrari, R. Vertical mixing, energy, and the general circulation of the oceans. *Annu. Rev. Fluid Mech.* **36**, 281–314 (2004).
- Wall, M., Schmidt, G. M., Janjang, P., Khokiattiwong, S. & Richter, C. Differential impact of monsoon and large amplitude internal waves on coral reef development in the Andaman Sea. *PLoS ONE* **7**, e50207 (2012).
- McWhorter, J. K. et al. The importance of 1.5 °C warming for the Great Barrier Reef. *Glob. Change Biol.* **28**, 1332–1341 (2022).
- Roder, C. et al. Metabolic plasticity of the corals *Porites lutea* and *Diploastrea heliophora* exposed to large amplitude internal waves. *Coral Reefs* **30**, 57–69 (2011).
- Wall, M. et al. Large-amplitude internal waves benefit corals during thermal stress. *Proc. Royal Soc. B: Biol. Sci.* **282**, 20140650 (2015).
- Storlazzi, C. D., Cheriton, O. M., van Hooijdonk, R., Zhao, Z. & Brainard, R. Internal tides can provide thermal refugia that will buffer some coral reefs from future global warming. *Sci. Rep.* **10**, 13435 (2020).
- Wijeratne, E. M. S., Woodworth, P. L. & Pugh, D. T. Meteorological and internal wave forcing of seiches along the Sri Lanka coast. *J. Geophys. Res.: Oceans* **115**. <https://doi.org/10.1029/2009JC005673> (2010).
- Jackson, C. R. & Apel, J. *An Atlas of Internal Solitary-like Waves and Their Properties* (Global Ocean Associates, 2004).
- Jensen, T. G. et al. Numerical modelling of tidally generated internal wave radiation from the Andaman Sea into the Bay of Bengal. *Deep Sea Res. Part II: Topical Studies Oceanography* **172**, 104710 (2020).
- Wang, Y.-H., Dai, C.-F. & Chen, Y.-Y. Physical and ecological processes of internal waves on an isolated reef ecosystem in the South China Sea. *Geophys. Res. Lett.* **34**, L18609 (2007).
- Villamaña, M. et al. Role of internal waves on mixing, nutrient supply and phytoplankton community structure during spring and neap tides in the upwelling ecosystem of Ría de Vigo (NW Iberian Peninsula). *Limnol. Oceanography* **62**, 1014–1030 (2017).
- Muacho, S., da Silva, J. C. B., Brotas, V. & Oliveira, P. B. Effect of internal waves on near-surface chlorophyll concentration and primary production in the Nazaré Canyon (west of the Iberian Peninsula). *Deep Sea Res. Part I: Oceanographic Res. Papers* **81**, 89–96 (2013).
- Saji, N. H., Goswami, B. N., Vinayachandran, P. N. & Yamagata, T. A dipole mode in the tropical Indian Ocean. *Nature* **401**, 360–363 (1999).
- McKenna, S., Santos, A., Gupta, A. S., Taschetto, A. S. & Cai, W. Indian Ocean Dipole in CMIP5 and CMIP6: characteristics, biases, and links to ENSO. *Sci. Rep.* **10**, 11500 (2020).
- Zuo, H., Balmaseda, M. A., Tietsche, S., Mogensen, K. & Mayer, M. The ECMWF operational ensemble reanalysis-analysis system for ocean and sea ice: a description of the system and assessment. *Ocean Science* **15**, 779–808 (2019).
- Hoyer, S. et al. xarray. <https://zenodo.org/record/6323468> (2022).
- Hoyer, S. & Hamman, J. xarray: N-D labeled arrays and datasets in Python. *J. Open Res. Softw.* **5**, 10 (2017).
- Rocklin, M. Dask: parallel computation with blocked algorithms and task scheduling. in *Proceedings of the 14th python in science conference*, Vol. 130 (Proceedings of the 14th Python in Science Conference, 2015).
- Abernathy, R. et al. xgcm/xgcm: v0.6.2rc1. <https://zenodo.org/record/6097129> (2022).
- Abernathy, R. et al. MITgcm/xmitgcm: v0.5.2. <https://zenodo.org/record/5139886> (2021).
- Zhuang, J. et al. pangeo-data/xESMF: v0.6.2. <https://zenodo.org/record/5721118> (2021).
- Busecke, J., Spring, A. & markusritschel. jbuscke/cmip6_preprocessing: v0.5.0rc4. <https://zenodo.org/record/5087632> (2021).
- Zheng, Q., Susanto, R. D., Ho, C.-R., Song, Y. T. & Xu, Q. Statistical and dynamical analyses of generation mechanisms of solitary internal waves in the northern South China Sea. *J. Geophys. Res.* **112**, C03021 (2007).
- Zhang, Z., Fringer, O. B. & Ramp, S. R. Three-dimensional, nonhydrostatic numerical simulation of nonlinear internal wave generation and propagation in the South China Sea. *J. Geophys. Res.: Oceans* **116**. <https://doi.org/10.1029/2010JC006424> (2011).
- Marshall, J., Adcroft, A., Hill, C., Perelman, L. & Heisey, C. A finite-volume, incompressible Navier Stokes model for studies of the ocean on parallel computers. *J. Geophys. Res.: Oceans* **102**, 5753–5766 (1997).
- 2021, G. B. C. G. The GEBCO_2021 Grid—a continuous terrain model of the global oceans and land. https://www.bodc.ac.uk/data/published_data_library/catalogue/10.5285/c6612cbe-50b3-0c0f-e053-6c86abc09f8f/ (2021).
- Yadidya, B., Rao, A. D. & Mohanty, S. Simulation of diurnal variability in vertical density structure using a coupled model. *Sci. Rep.* **11**, 10916 (2021).
- Smagorinsky, J. General circulation experiments with the primitive equations: i. the basic experiment. *Monthly Weather Rev.* **91**, 99–164 (1963).
- Egbert, G. D. & Erofeeva, S. Y. Efficient inverse modeling of barotropic ocean tides. *J. Atmos. Oceanic Technol.* **19**, 22 (2002).
- Niwa, Y. & Hibiya, T. Three-dimensional numerical simulation of M2 internal tides in the East China Sea. *J. Geophys. Res.: Oceans* **109**. <https://doi.org/10.1029/2003JC001923> (2004).

58. Nash, J. D., Alford, M. H. & Kunze, E. Estimating internal wave energy fluxes in the ocean. *J. Atmos. Oceanic Technol.* **22**, 1551–1570 (2005).
59. Wang, X. et al. Tidal mixing in the south china sea: an estimate based on the internal tide energetics. *J. Phys. Oceanography* **46**, 107–124 (2016).
60. Vic, C. et al. Deep-ocean mixing driven by small-scale internal tides. *Nat. Commun.* **10**, 2099 (2019).

Acknowledgements

The authors like to express their gratitude to the Indian Institute of Technology Delhi HPC (High-Performance Computing) facility and the Government of India's Department of Science and Technology (DST) for authorising financial grants for computational resources (DST-FIST, 2014). The first author wishes to express his gratitude to the DST, New Delhi, for financial support in the form of the INSPIRE research fellowship.

Author contributions

B.Y.: conceptualisation, methodology, model simulations, formal analysis, figures and manuscript writing. A.D.R.: conceptualisation and manuscript review.

Competing interests

The authors declare no competing interests.

Additional information

Supplementary information The online version contains supplementary material available at <https://doi.org/10.1038/s43247-022-00574-8>.

Correspondence and requests for materials should be addressed to B. Yadidya.

Peer review information *Communications Earth & Environment* thanks the anonymous reviewers for their contribution to the peer review of this work. Primary Handling Editors: Viviane V. Menezes and Clare Davis. Peer reviewer reports are available.

Reprints and permission information is available at <http://www.nature.com/reprints>

Publisher's note Springer Nature remains neutral with regard to jurisdictional claims in published maps and institutional affiliations.



Open Access This article is licensed under a Creative Commons Attribution 4.0 International License, which permits use, sharing, adaptation, distribution and reproduction in any medium or format, as long as you give appropriate credit to the original author(s) and the source, provide a link to the Creative Commons license, and indicate if changes were made. The images or other third party material in this article are included in the article's Creative Commons license, unless indicated otherwise in a credit line to the material. If material is not included in the article's Creative Commons license and your intended use is not permitted by statutory regulation or exceeds the permitted use, you will need to obtain permission directly from the copyright holder. To view a copy of this license, visit <http://creativecommons.org/licenses/by/4.0/>.

© The Author(s) 2022